

Role of the compensating current in the weak Josephson coupling regime: An extended study on excitonic Josephson junctions

Ya-Fen Hsu^{1,2,*} and Jung-Jung Su^{2,†}

¹*Physics Division, National Center for Theoretical Science, Hsinchu, 30013, Taiwan*

²*Department of Electrophysics, National Chiao Tung University, Hsinchu 300, Taiwan*

(Dated: December 8, 2020)

Huang’s experiment [Phys. Rev. Lett. **109**, 156802 (2012)] found, in the quantum Hall bilayer of the Corbino geometry, the interlayer tunneling currents at two edges are coupled to each other and one of two tunneling currents is referred to as the compensating current of the other. The recent theoretical work [arXiv:2006.15329] has explained this exotic coupling phenomenon as a result of excitonic Josephson effect induced by interlayer tunneling current. In this paper, we study the same setup—excitonic Josephson junction—but in the weak Josephson coupling regime, which occurs for large junction length. Interestingly, we find the compensating current drives the other edge to undergo a nonequilibrium phase transition from a superfluid to resistive state, which is signaled by an abrupt jump of the critical tunneling current. We also identify the critical exponent and furthermore offer more experimental prediction.

I. INTRODUCTION

Josephson effect is particularly attractive to condensed matter researchers because it serves as the striking manifestation of coherent condensation and the promising candidate for quantum technology. The unrelenting and strong attention has been received recently in optically-excited exciton or exciton-polariton cold gases^{1–7} and graphene electron-hole bilayer exciton^{8,9}. However, being the best platform to achieve the exciton condensation, the quantum Hall bilayer^{10–33} remains not studied extensively in the land of Josephson effect. Actually, the search for Josephson effect in quantum Hall bilayer ever arouse intense interest since the observation of Josephson-like tunneling^{34,35}, in which the interlayer voltage abruptly increases once exceeding a critical tunneling current^{12,15,19,21,23,26}. However, to the end, the Josephson-like tunneling is attributed to a mixture of coherent and incoherent interlayer tunneling^{36–38} instead of the “real” Josephson effect. Once exceeding a critical current, the incoherent tunneling dominates over the coherent one.

The scattering approach by solving the Bogolubov-de Gennes Hamiltonian^{39–41} is the standard one to explore the Josephson effect but it is difficult to access in the context of quantum Hall bilayer. In our previous works^{42,43}, we therefore turn to a new method within the frame of pseudospin dynamics based on the idea that the layers can be treated as pseudospin quantum degrees of freedom^{38,44,45}. We firstly employ this new method to study the exciton-condensate/exciton-condensate (EC/EC)⁴² and exciton-condensate/normal-barrier/exciton-condensate (EC/N/EC) junctions⁴³ with a constant relative phase between two ECs that is generated by perpendicular electric field⁴⁶. We found that excitonic Josephson effect occurs only when $d_J \leq \xi$, where d_J and ξ are barrier length and correlation length^{42,43}. When $d_J > \xi$, a new transport mechanism, namely, tunneling-assisted Andreev reflection occurs at a single

N/EC interface⁴³. While the excitonic Josephson effect gives rise to novel fractional solitons⁴², the new mechanism leads to a half portion of fractional solitons⁴³. Notably, these new types of solitons have potential to improve the stability and efficiency of quantum logic circuits⁴⁷. We next study another setup suggested to have a relative phase by externally applying interlayer tunneling current⁴⁸.

Inspired by Huang’s experiment⁴⁹, we consider the setup of interlayer tunneling currents exerted on two edges of quantum Hall bilayer as shown in Fig. 1(a). The tunneling currents (J_{tL}, J_{tR}) twist the condensate phases of two edges so as to create the relative phases between three condensates: EC1, EC2, and EC3. Such structure is regarded as two condensates (EC1 and EC3) sandwiched by a superfluid barrier (EC2), which is a type of excitonic Josephson junctions⁵¹. Ref.⁵⁰ has explored this setup but focuses on the short junction whose junction length L is smaller than Josephson length λ ⁵². Its results demonstrated that the exotic coupling phenomenon of edge tunneling currents observed by Huang *et al*⁴⁹ is originated from excitonic Josephson effect and Huang’s experiment is a very robust evidence for quantum Hall bilayer exciton condensation.

In this paper, we turn our attention to the opposite case—the long junction of $L \sim 10\lambda$, which corresponds to the typical quantum Hall bilayer^{12,57}. Our calculation of the condensate phase [see Fig. 1(b)] reflects that the Josephson current is essentially negligible in the bulk since the phase goes to zero and becomes flat there⁵⁸. Because the two edges are weakly Josephson coupled, the long junction can be approximated as two independent EC/EC junctions with the boundary between them occurring where Josephson current J_s goes to zero [see the inset of Fig. 1(b)]. It is therefore highly desirable that the long junction can display entirely different properties from the short junction in which two edges are strongly Josephson coupled⁵⁰.

It turns out that the long junction indeed exhibits an

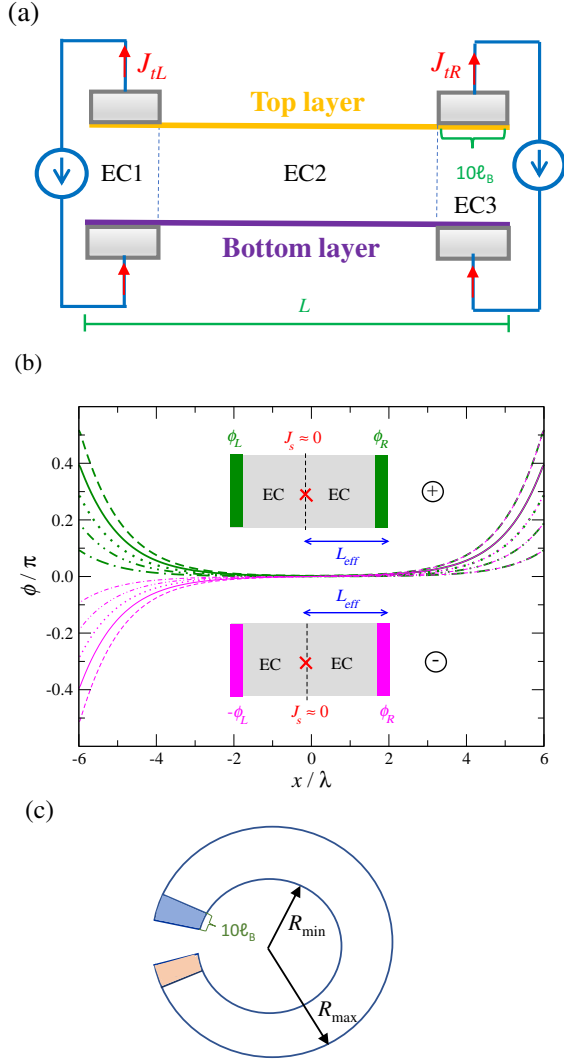


FIG. 1. (color online) (a) Schematic layout of an excitonic Josephson junction induced by interlayer tunneling current. The relative phases between three condensate regions: EC1, EC2 and EC3, are generated by externally applying tunneling currents J_{tL} and J_{tR} . ℓ_B and L denote the magnetic and junction length. (b) The calculated phase distributions for parallel polarity \oplus ($J_{tL} = J_{tR}$) and anti-parallel polarity \ominus ($J_{tL} = -J_{tR}$) with $L = 12\lambda$. The green (black) and pink (grey) lines correspond to the parallel and anti-parallel polarity, respectively. The employed values of J_{tR} are 5, 10, 15, 20, 25 J_{t0} and with increasing J_{tR} , the phase ϕ departs from the x axis. The length unit λ and the current unit J_{t0} are given later in Sec. II C. Such a long junction is similar to two weakly coupled exciton-condensate/exciton-condensate (EC/EC) junctions. The cross is the breakpoint between two EC/EC junctions and it is located where the Josephson current J_s approaches zero. The left (right) part of the bulk combines with the left (right) edge forming an EC/EC junction. L_{eff} denotes the effective junction length of the right EC/EC junction. (c) Schematic layout of a Corbino-geometry excitonic Josephson junction. The two tunneling currents J_{tL} and J_{tR} are exerted on the orange (lower) and blue (upper) shadow zones. R_{min} and R_{max} are the minimum and maximum radius.

unique property: one edge undergoes a nonequilibrium phase transition^{53,54} with increasing the tunneling current at the other edge (i.e., the compensating current). During this phase transition, the critical tunneling current of the edge sharply falls and the corresponding critical exponent is identified as $\gamma \sim 0.5$. Since the Josephson coupling is weak, we wonder why the compensating current can influence the other edge so largely? According to our analysis, this is because the compensating current reduces the effective junction length of the constituent EC/EC junction on the opposite side. We furthermore calculate the magnetic field induced by Josephson current (denoted by B_J) for the Corbino-geometry excitonic Josephson junction shown in Fig. 1(c). We find the length reduction effect is revealed by the crossover of the B_J versus ΔJ_t curve into the short junction regime⁵⁰ (a linear one) with increasing the compensating current, where $\Delta J_t = J_{tR} - J_{tL}$. The induced magnetic field is estimated at ~ 100 pT that is large enough to be detected by the scanning superconducting interference device (SQUID). In the main body of this paper, we show the results of the rectangle-shaped junction in Figs. 3-7 while that of the Corbino-geometry junction in Figs. 8-9.

II. MODEL AND METHOD

Burkov and MacDonald treated two layers of the quantum Hall bilayer as pseudospin quantum degrees of freedom and accordingly deduced a lattice model Hamiltonian⁴⁵:

$$H = \frac{1}{2} \sum_{ij} (2H_{ij} - F_{i,j}^{\text{intra}}) S_i^z S_j^z - F_{i,j}^{\text{inter}} (S_i^x S_j^x + S_i^y S_j^y),$$

$$\vec{S}_i = \frac{1}{2} \sum_{\sigma, \sigma'} a_{i,\sigma}^\dagger \vec{\tau}_{\sigma, \sigma'} a_{i,\sigma'}. \quad (1)$$

Here $a_{i,\sigma}^\dagger$ ($a_{i,\sigma}$) is the Schwinger boson creation (annihilation) operators⁵⁵ where i and σ label the site and layer indexes and $\vec{\tau}$ is the Pauli matrix vector. The Hartree term H_{ij} describes the direct Coulomb interaction while the Fock term $F_{i,j}^{\text{intra}}$ ($F_{i,j}^{\text{inter}}$) serves the intralayer (interlayer) exchange interaction. This lattice Hamiltonian possesses eigenstate wave function which can be generally expressed as

$$|\Psi\rangle = \prod_i \left[\cos \frac{\theta(\vec{X}_i)}{2} c_{i\uparrow}^\dagger + \sin \frac{\theta(\vec{X}_i)}{2} e^{i\phi(\vec{X}_i)} c_{i\downarrow}^\dagger \right] |0\rangle. \quad (2)$$

The operator $c_{i\uparrow}^\dagger$ ($c_{i\downarrow}^\dagger$) creates an electron at the lattice site location \vec{X}_i in the top (bottom) layer. It is difficult to study the present issue through quantum scattering approach which is based on this wave function since we cannot simply write down the explicit forms of $\theta(\vec{X}_i)$ and $\phi(\vec{X}_i)$.

We therefore request a SU(2) to O(3) mapping and the wave function is transformed into a classical pseudospin⁴⁴

$$\begin{aligned} \vec{m}(\vec{X}_i) &= (m_\perp \cos \phi, m_\perp \sin \phi, m_z), \\ m_\perp &= \sin \theta, m_z = \cos \theta. \end{aligned} \quad (3)$$

Accordingly, the dynamics of the quantum Hall bilayer can be described by the Landau-Lifshitz-Gilbert (LLG) equation^{38,42,43}

$$\begin{aligned} \frac{d\vec{m}}{dt} &= \vec{m} \times (2/n\hbar)(\delta E[\vec{m}]/\delta \vec{m}) - \alpha \left(\vec{m} \times \frac{d\vec{m}}{dt} \right), \\ E[\vec{m}] &= A_{\text{unit}} \sum_i \left[\beta m_z^2 + \frac{\rho_s m_\perp^2}{2} |\nabla_{\vec{X}_i} \phi|^2 \right. \\ &\quad \left. - \frac{n\Delta_t m_\perp}{2} \cos \phi \right], \end{aligned} \quad (4)$$

where A_{unit} is the area of the unit cell for the pseudospin lattice and n is the pseudospin density. The excitonic superfluid loses its coherence after traveling over one correlation length ξ so the size of the unit cell is equal to ξ , which is estimated at $\sim 200\text{nm}$ ⁵⁶. In unit of the magnetic length l_B , $\xi \sim 10l_B$ (l_B has the typical value of $\sim 20\text{nm}$). On the other hand, the energy functional $E[\vec{m}]$ is composed of the capacitive penalty, the exchange correlation, and the interlayer tunneling energy, which are characterized by the parameters: anisotropic energy β , pseudospin stiffness ρ_s , and single-particle tunneling Δ_t , respectively. These model parameters is up to which kind of samples we are discussing. The second term for the LLG equation is the Gilbert damping which relaxes the energy toward the minimum.

A. Modeling excitonic Josephson junctions

The key breakthrough of the present work is to introduce the effect of external tunneling currents. When exerting the $+\hat{z}$ -direction tunneling current J_t on a area of A over a short duration of dt , there are electrons as many as $J_t A dt/e$ pouring out of the top layer and trickling into the bottom layer simultaneously (see Fig. 2), giving rise to the change of $-2J_t A dt/e$ in the total pseudospin nAm_z . Under the effect of tunneling current, the z -component LLG equation thus can be modified as

$$\frac{dm_z}{dt} = -\frac{2\rho_s}{n\hbar} m_\perp^2 \nabla^2 \phi + \frac{\Delta_t}{\hbar} m_\perp \sin \phi - \frac{2J_t}{ne} + \alpha m_\perp^2 \frac{d\phi}{dt}. \quad (5)$$

In the rectangle-shaped excitonic Josephson junction as shown in Fig. 1(a), two tunneling current J_{tL} and J_{tR} are applied to two edges over a length as large as one lattice size $10l_B$. We can therefore model the junction through setting J_t to

$$\begin{aligned} J_t &= J_{tL} \Theta(x + L/2) \Theta(L/2 - 10l_B - x) \\ &\quad + J_{tR} \Theta(L/2 - x) \Theta(x - L/2 + 10l_B). \end{aligned} \quad (6)$$

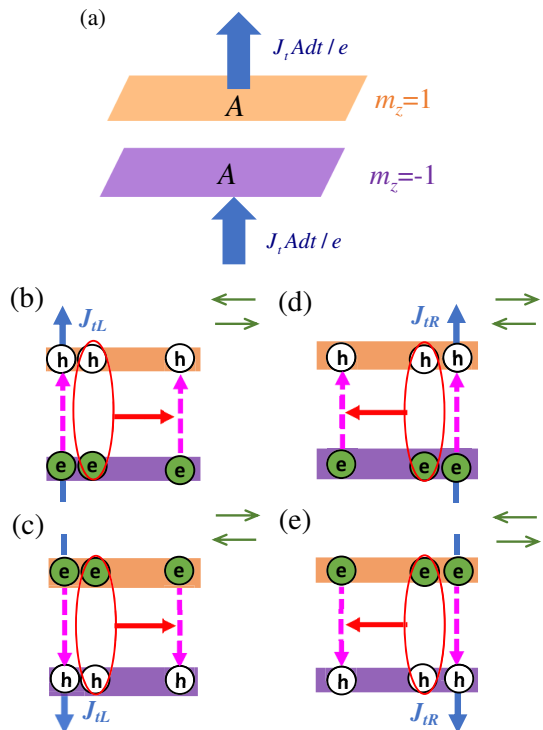


FIG. 2. (color online) (a) Illustration of the effect of external tunneling current J_t . Here the top and bottom layers are selected as up pseudospin ($m_z = 1$) and down pseudospin ($m_z = -1$). The notation A denotes the area that tunneling current passes through. Over the time duration dt , the electrons number that flows out of the top layer or flows into the bottom layer is counted by $J_t A dt/e$. (b),(c) and (d),(e) depict the flows of electrons and excitons when applying the external tunneling current to the right and left edges, respectively. The solid red and dashed pink arrows indicate the direction of exciton flow and single-particle tunneling, respectively. The insets at their upper right corner are the individual corresponding counterflow currents. For convenience in discussion, we choose $+e$ as the charge of an electron and e is actually a negative amount. The current therefore goes along the flow direction of electrons.

Notice we from here on use the continuous varying x instead of the discrete X_i for convenience in presentation and $\Theta(x)$ is the Heaviside step function. The origin $x = 0$ is defined to be located at the center of the junction. After evolving with time, we ultimately acquire the static solutions for ϕ , m_\perp , and m_z that specify the pseudospin orientation. The counterflow Josephson current is furthermore calculated by

$$J_s = e\rho_s \nabla \phi / \hbar. \quad (7)$$

The physical picture for the effect of external tunneling currents can be depicted through Figs. 2(b)-(e). When applying the $+\hat{z}$ -direction tunneling current to the left edge [see Fig. 2(b)], holes and electrons are injected into the top and bottom layer from the left side, respectively. The electrons can flow into the top layer to annihilate

holes via single-particle tunneling Δ_t or combine with holes to form excitons $|h \uparrow; e \downarrow\rangle$ and then transmit right into the junction bulk, where $|h \uparrow; e \downarrow\rangle$ indicates a state composed of a hole in the top layer bound to an electron in the bottom layer. However, single-particle tunneling destroys the excitons everywhere and leads to the attenuation of counterflow Josephson current in the bulk. When reversing the direction of external tunneling current [see Fig. 2(c)], the roles of electrons and holes are exchanged and right-going but opposite polarized excitons $|e \uparrow; h \downarrow\rangle$ occur, where $|e \uparrow; h \downarrow\rangle$ indicates a state composed of an electron in the top layer bound to a hole in the bottom layer. Similarly, applying the $+\hat{z}(-\hat{z})$ -direction tunneling current to the right edge will generate “left”-going excitons $|h \uparrow; e \downarrow\rangle$ ($|e \uparrow; h \downarrow\rangle$) [see Figs. 2(d)-(e)]. It turns out that the external tunneling currents with parallel (anti-parallel) polarity will inject counterflow Josephson current in the opposite (same) direction as shown in the

insets of Figs. 2(b)-(e).

B. Calculation of induced magnetic field due to excitonic Josephson effect

We next consider a Corbino-geometry excitonic Josephson junction that can generate circular Josephson current [see Fig. 1(c)]. The Corbino can be divided into a set of rings with radius which ranges from R_{\min} to R_{\max} . A single ring of the specific radius r can be viewed as a bent Josephson junction with $L = 2\pi r$. We firstly calculate the phase distribution for the junction of $L = 2\pi R_{\min}$ by the LLG equation and then acquire the phase distribution for other values of r by taking the azimuthal symmetry into account. The Josephson current is similarly calculated by Eq. (7). By using the Biot-Savart Law, we finally obtain the induced magnetic field:

$$B_J(z) = \frac{\mu_0 \langle J_s(R_{\min}, \theta) \rangle_\theta z d R_{\min}}{2} \left[\frac{1}{(R_{\min}^2 + z^2)^{3/2}} - \frac{1}{(R_{\max}^2 + z^2)^{3/2}} \right], \quad (8)$$

where d is the interlayer separation, z is the distance above the center of the bilayer, and $\langle \dots \rangle_\theta$ is the average over the angular axis of polar coordinate.

C. Choice of units, identification of critical current and determination of parameters

Both two geometries we consider are discussed based on a length scale, namely, Josephson length:

$$\lambda = \sqrt{2\rho_s/n\Delta_t}. \quad (9)$$

Two units for Josephson current and tunneling current read $J_{s0} = e\rho_s/\hbar\lambda$ and $J_{t0} = en\Delta_t/2\hbar$ throughout this paper. We identify the critical interlayer tunneling current by finding the upper and lower boundaries at which the junction departs from the coherent state, i.e., m_z begins to become nonzero. The main focus of the present work is the typical quantum Hall bilayer of $\lambda \sim 45\mu\text{m}$ ($\Delta_t = 10^{-8}E_0$)⁵⁷, which corresponds to the samples fabricated by Eisenstein’s group¹². Here the Coulomb interaction $E_0 = e^2/\epsilon l_B$ serves as the energy scale and $E_0 \sim 7\text{meV}$. The other parameters we use are listed as follows: $\beta = 0.02E_0$ and $\rho_s = 0.005E_0$, which were derived from the mean-field calculation⁵⁷.

III. ANALYSIS OF ROLE OF THE COMPENSATING CURRENT

Figs. 3(a)-(b) show that edge-state currents inevitably contribute to the coupling of the left and right edges for the Hall-bar geometry while two edge-state currents separately flow along the inner and outer boundaries so as not to connect the left and right edges for the Corbino geometry²⁴. To avoid the contribution of edge-state currents, Fig. 3(b) is the main setup we consider here and its corresponding junction length roughly approximates to the difference of the inner and outer radius. The realistic Corbino geometry possesses the junction length $L \sim 0.54\text{mm}$ ⁴⁹ and in the context of the typical quantum Hall bilayer¹² ($\lambda = 45\mu\text{m}$), the junction length reads $L \sim 12\lambda$. The large part of this paper therefore focuses on the case of $L = 12\lambda$ later.

A. Nonequilibrium phase transition

The realization of the short junction with $L = 0.6\lambda$ ⁵⁰ — Huang’s experiment⁴⁹ — is devoted to analyzing Josephson-like behavior, in which the interlayer voltage suddenly emerges when applying tunneling current up to critical values: the upper and lower I^c [see Fig. 3(c)]. They found the upper and lower critical currents are correlated with its compensating current — the tunneling current exerted on the other edge and such coupling of the tunneling currents at two edges would disappear

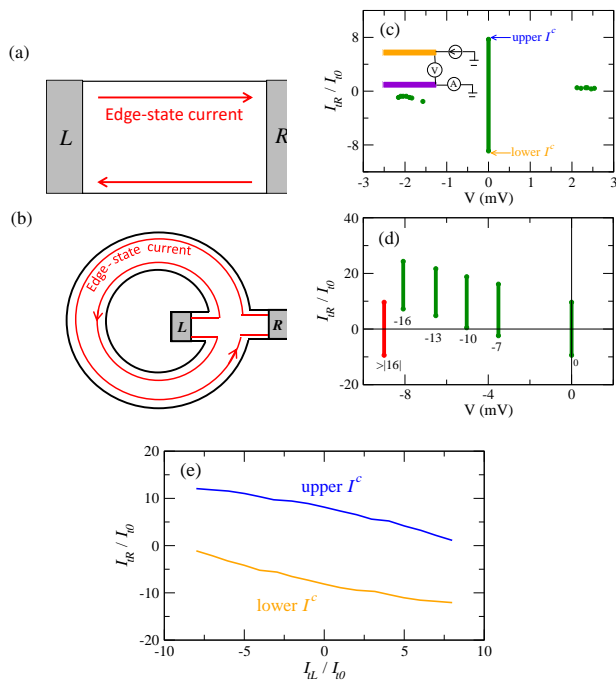


FIG. 3. (color online) (a) and (b) depict the junction geometry: (a) the standard Hall bar geometry and (b) the Corbino geometry. (c)-(e) summarize the key results of Huang's experiment (a realization of short Josephson junction): (c) Josephson-like I - V characteristic without the compensating current applied. The inset shows the measurement configuration. (d) Josephson-like I - V characteristic for different values of the compensating current. The numbers below the traces labels the corresponding value of the compensating current I_{tL}/I_{t0} . The I - V curves are offset by $(I_{tL}/2I_{t0})mV$. (e) The critical currents as a function of the compensating current. The measured current $I_{tL(R)} = J_{tL(R)}A$ and the unit $I_{t0} = 1nA$, where A labels the effective cross area of external tunneling currents. A is difficult to determine through the existing experimental information. The data of (c)-(e) are reproduced from Ref.⁴⁹.

when $|I_{tL}| > 16nA$ [see Fig. 3(d)]. The disappearance phenomenon will be discussed later in Sec. IV A and we focus on how the tunneling currents at two edges correlate with each other here. Huang's experiment quantifies this coupling through the plot of the critical currents as function of the compensating current [see Fig. 3(e)]. Therefore, we also display the similar plot for the long junction in Fig. 4 to analyze the role of the compensating current. Over a wide range of J_{tL} , the upper and lower critical currents nearly keep constant and are symmetric with respect to $J_{tR} = 0$ [see Fig. 4(a)]. Near $J_{tL} = \pm 30.692J_{t0}$, however, the critical currents rapidly fall to zero. The sharp jump of critical currents J^c indicates the right edge is switched from a superfluid to resistive state. The right edge undergoes a phase transition under the condition of compensating-current-driven nonequilibrium^{53,54}. With slowly adjusting J_{tL} , it is identified as a first-order phase transition since $|J^c(J_{tL} = \pm 30.692J_0)| = 15.999J_0$ and $|J^c(J_{tL} =$

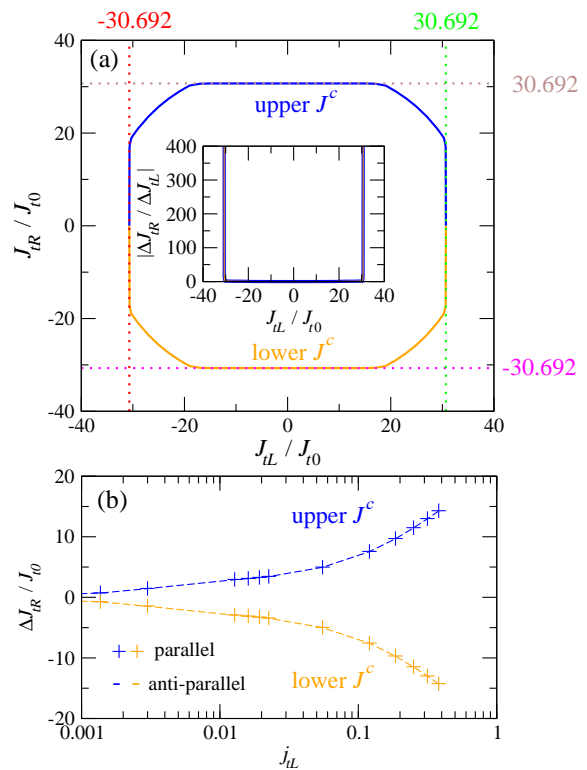


FIG. 4. (color online) (a) The calculated upper and lower critical values of the external tunneling current J_{tR} as a function of its compensating current J_{tL} . The inset: the corresponding slopes $\Delta J_{tR} / \Delta J_{tL}$ as a function of J_{tL} . (b) The identification of critical exponents near two phase transition points occurring at $J_{tL} = \pm 30.692J_{t0}$. Here $\Delta J_{tR} = J^c(J_{tL}) - J^c(\pm 30.692J_{t0})$ and $j_{tL} = |(J_{tL} - \pm 30.692J_{t0}) / \pm 30.692J_{t0}|$. The choice of \pm is up to which phase transition point we are discussing. By fitting to the numerical results presented in this figure, we extract the exponent γ , which is defined as $\Delta J_{tR} \propto j_{tL}^\gamma$, and find $\gamma \sim 0.5$ for any phase transition point.

$\pm 30.6925J_0)| = 0$ (The giant change in critical currents hints possible discontinuity). We furthermore define new critical exponents:

$$\Delta J_{tR} \propto \begin{cases} (30.692J_{t0} - J_{tL})^{\gamma^+} & \text{for } J_{tL} \lesssim 30.692J_{t0}, \\ (J_{tL} + 30.692J_{t0})^{\gamma^-} & \text{for } J_{tL} \gtrsim -30.692J_{t0}, \end{cases} \quad (10)$$

where $\Delta J_{tR} = J^c(J_{tL}) - J^c(\pm 30.692J_{t0})$. The fits to our numerical results extract the values of exponents [see Fig. 4(b)]: $\gamma^+ = 0.4939$, $\gamma^- = 0.4999$ for the upper J^c curve. For the lower J^c curve, the values of γ^+ and γ^- are exactly exchanged because of electron-hole symmetry.

B. Junction-length reduction effect

Why the compensating current can largely reduce the critical currents as $J_{tL} \approx \pm 30.692J_{t0}$ even if the Josephson coupling is so weak? As have been illustrated in Fig. 1(b), the long junction can be decomposed into two

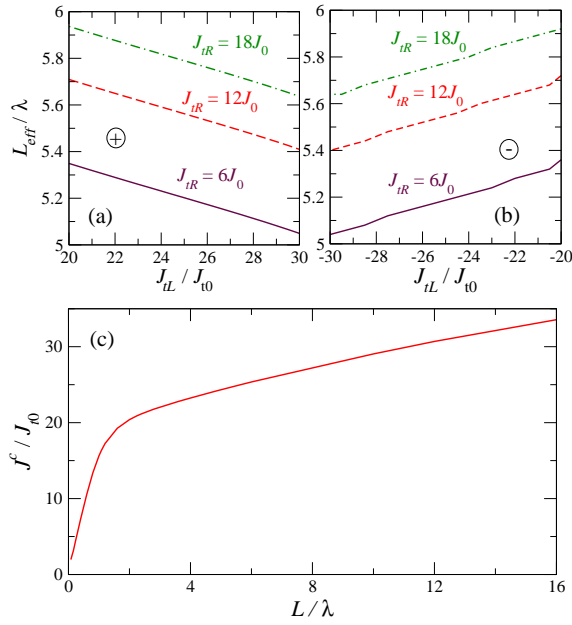


FIG. 5. (color online) (a) and (b) are the effective length of the right EC/EC junction as a function of the corresponding compensating current J_{tL} for the parallel polarity \oplus and anti-parallel polarity \ominus with the right tunneling current $J_{tR} = 6, 12, 18J_{t0}$. (c) The junction-length dependence of critical current J^c without the compensating current applied ($J_{tL} = 0$).

nearly independent EC/EC junctions. We here identify the breakpoint occurring at $J_s = 0$ or where J_s reaches its minimum and determine the effective length of the right EC/EC junction as shown in Figs. 5(a)-(b). We find, regardless of the polarity, the compensating current J_{tL} decreases the effective length of the right junction and hence leads to the jump of the critical currents. It is quite intuitive or shown in Fig. 5(c) that the critical current would decrease with decreasing the junction length.

IV. OTHER INTERESTING PREDICTION

A. Discussion on Josephson breakdown effect

Now let us turn our attention to the disappearance phenomenon of the coupling of the two edge tunneling currents shown in Fig. 3(b) occurring as $|I_{tL}| > 16nA$. For this disappearance phenomenon, the main body of Ref.⁴⁹ furthermore demonstrates that it is accompanied with the occurrence of the interedge voltage. Ref.⁵⁰ has attributed this phenomenon to the breakdown of Josephson effect— when Josephson current attains some critical value, the Josephson effect would collapse and the external tunneling currents will prefer to converting into edge-state currents. We here comment on whether this breakdown effect occurs also in the long junction or not.

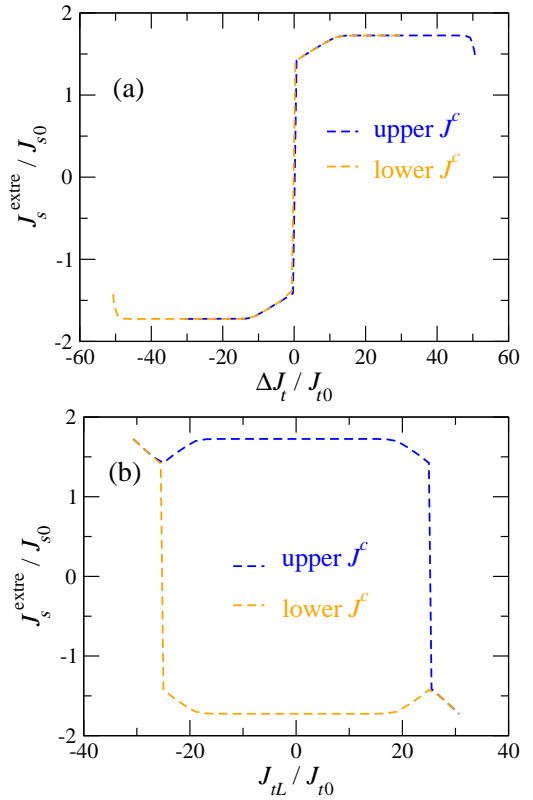


FIG. 6. (color online) The spatial extrema of Josephson current J_s^{extre} as a function of (a) the difference of two tunneling currents $\Delta J_t = J_{tR} - J_{tL}$ and (b) the compensating current J_{tL} for the upper and lower critical points of J_{tR} .

Differing from the short junction, the upper and lower J^c curves are always symmetric with respect to $J_{tR} = 0$ as if the Josephson breakdown effect already happens and the applied compensating current is limited to a range of $J_{tL} = -30.692J_{t0} \sim 30.692J_{t0}$ beyond which coherent interlayer tunneling disappears [see Fig. 4(a)]. We have performed numerical calculation demonstrating that over the range of $J_{tL} = -30.692J_{t0} \sim 30.692J_{t0}$, static solutions can exist and there was not found any critical variation. We therefore believe that the breakdown effect does not occur in the long junction.

We furthermore give more detail analysis through Fig. 6. The difference of external tunneling currents ΔJ_t plays the similar role as the relative phase in the conventional Josephson junction⁵¹ while it is easier to compare with the experiment directly based on the compensating current J_{tL} . In Fig. 6, we therefore plot the spatial extrema of Josephson current J_s^{extre} as a function of not only ΔJ_t but also J_{tL} . We find that J_s^{extre} rises or drops to saturation over the range of $\Delta J_t = 20J_{t0} \sim 40J_{t0}$ or $\Delta J_t = -20J_{t0} \sim -40J_{t0}$ [see Fig. 6(a)], which corresponds to $J_{tL} = -20J_{t0} \sim 20J_{t0}$ [see Fig. 6(b)]. With increasing the compensating current, if the Josephson-breakdown regime is achieved, it necessarily occurs at $J_{tL} = -20J_{t0} \sim 20J_{t0}$ where the J^c curves hold horizon-

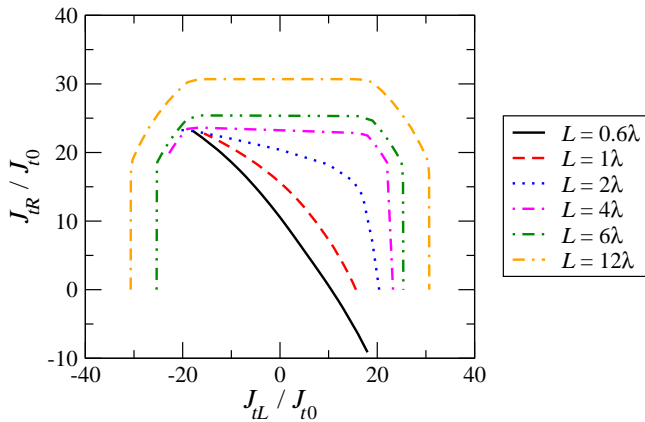


FIG. 7. (color online) The critical value of the external tunneling current J_{tR} versus the compensating current J_{tL} for different junction length L .

tal [see Fig. 4(a)]. Measuring the interedge voltage will help us clarify the junction being in the weak Josephson coupling regime or Josephson-breakdown regime. Alternatively, after increasing the compensating current beyond $\pm 20J_{t0}$, $|J^c|$ begins to fall [see Fig. 4(a)], providing an unique signature for the weakly Josephson coupling, namely, Josephson fall.

B. The crossover behavior with varying junction length

Since the dependence of the critical currents on the compensating current is so distinct for the short and long junctions, we next want to understand the crossover behavior with increasing junction length through Fig. 7. Because the lower J^c curve can be produced through doing the electron-hole transformation: $J_{tR} \rightarrow -J_{tR}$, $J_{tL} \rightarrow -J_{tL}$ on the upper J^c curve, in Fig. 7, we display only the upper J^c curve for conciseness. Fig. 7 shows that, with increasing the junction length, the curve is gradually skew and no abrupt change occurs. Moreover, the Josephson fall already can be found as $L = 4\lambda$ while the weakly “symmetric” Josephson regime can be achieved as $L \sim 5\lambda$. The values of 5λ happens to meet the junction length for the typical quantum Hall bilayer¹² of Hall-bar geometry ($L \sim 225\mu\text{m}$) but the Hall-bar geometry may be difficult to coincide with our calculation due to the influence of edge-state current. Replacing the usually-used side electrodes with the top and back electrodes would be a method to avoid edge-state currents although it is a big technological challenge.

C. The induced magnetic field due to Josephson current in a Corbino geometry

Next Fig. 8 shows the results for the Corbino-geometry excitonic Josephson junction, which is depicted in Fig.

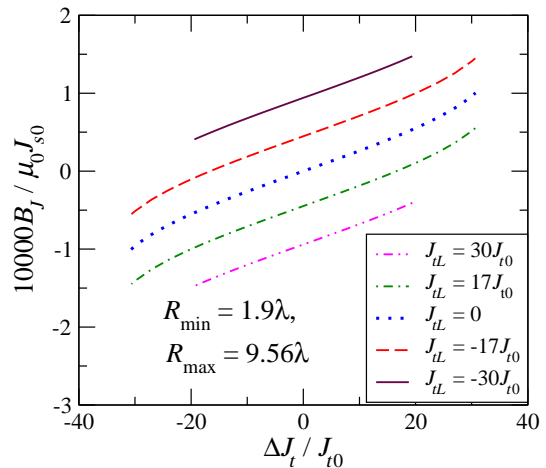


FIG. 8. (color online) The induced magnetic field B_J due to circular Josephson current of a Corbino-geometry excitonic Josephson junction at $z = 2.22\lambda$ as a function of the difference of two external tunneling currents $\Delta J_t = J_{tR} - J_{tL}$ for $R_{\min} = 1.9\lambda$ and $R_{\max} = 9.56\lambda$. The curves are offset by the corresponding J_{tL} . The interlayer separation $d = 1.6\ell_B$, where ℓ_B is the magnetic length.

1(c) (the curves is offset by the corresponding compensating current for clarity and a without-offset version is given in Appendix A). In Fig. 8, except for the minimum radius R_{\min} , the other parameters are determined according to the realistic situation of experiments. The minimum radius for the typical Corbino is roughly 0.16mm or equivalently $R_{\min} \sim 3.56\lambda$ instead of $R_{\min} = 1.9\lambda$ that we choose for increasing the numerical efficiency. But, the investigated Corbino of $\lambda < 2\pi R_{\min} < 2\pi R_{\max}$ can already capture the physics of the long junction to a qualitative level and such a Corbino with smaller R_{\min} is easily realized by etching. We find, differing from the short junction⁵⁰, the dependence of the induced magnetic field B_J on the difference of two tunneling currents ΔJ_t can have apparent curvature. The curve however becomes linear when J_{tL} reaches $\pm 30J_{t0}$. This is because J_{tL} decreases the effective length of the EC/EC junction on the opposite side and drives the investigated Corbino into the short-junction regime of a linear dependence⁵⁰. Moreover, the extremely subtle magnetic field must be measured by the scanning superconducting quantum interference device (SQUID). To our best knowledge, the resolution of the typical scanning SQUID is up to $\sim 10\text{pT}$ at a sensor-to-sample distance of $\sim 100\text{nm}$ and the current technology even improves the resolution to $\sim 1\text{pT}$ ⁵⁹. We estimate B_J on the scale $\sim 100\text{pt}$ and it is measurable without doubt.

V. CONCLUSION

In conclusion, we predict a nonequilibrium phase transition occurring in the long junction of weak Josephson

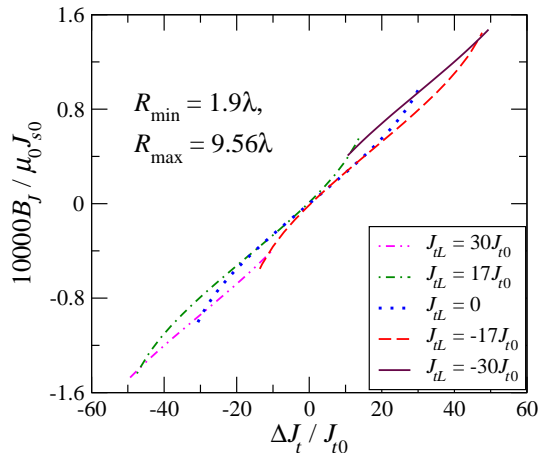


FIG. 9. (color online) The without-offset version for Fig. 8, where B_J and ΔJ_t denote the induced magnetic field and the difference of two external tunneling currents, respectively.

coupling and find the effective length reduction effect of the compensating current. The sample size is not highly tunable in experimental measurement and therefore this length reduction effect will be largely helpful in observing the interesting crossover behavior predicted in Ref.⁴³. We furthermore discuss the possibility of the breakdown of Josephson effect and suggest measuring the interedge voltage and Josephson fall⁶⁰ to distinguish the Josephson breakdown effect from weak Josephson coupling. We also calculate the induced magnetic field in the Corbino-geometry Josephson junction to suggest the detection of Josephson current. It should be noted that there are still very much theoretical effort called for, such as de-

veloping Bogolubov-deGennes description, exactly identifying phase transition (especially for it being first-order or second-order), systematically exploring the Josephson breakdown effect and etc. We believe the present work together with Ref.⁵⁰— excitonic Josephson effect induced by interlayer tunneling current—will bring new attention to the condensed matter physics community.

ACKNOWLEDGE

We are grateful to W. Dietsche, A. H. MacDonald, B. Rosenstein, Jheng-Cyuan Lin, Sing-Lin Wu and Chien-Ming Tu for valuable discussion. This work were financially supported by Ministry of Science and Technology and by National Center for Theoretical Sciences of Taiwan.

APPENDIX A: THE WITHOUT-OFFSET VERSION FOR FIG. 8

In Fig. 9, we display the original curves of Fig. 8, being not offset, to capture more definite understanding for the ΔJ_t dependence. Similar to the short junction discussed in Ref.⁵⁰, the curves for different J_{tL} approaches each other but apparent derivation exists for large ΔJ_t . That is to say, for the long junction, the magnitude of the induced magnetic is dependent on not only the difference of two external edge tunneling currents but also their individual values, which can be regarded as a characteristic of weak Josephson coupling. This is because in the weakly Josephson-coupled regime, the edge property becomes prominent.

* E-mail address: yafen.hsu.jane@gmail.com

† E-mail address: jungjsu@nctu.edu.tw

- [1] M. Wouters and I. Carusotto, *Phys. Rev. Lett.* **99**, 140402 (2007).
- [2] I. A. Shelykh, D. D. Solnyshkov, G. Pavlovic and G. Malpuech, *Phys. Rev. B* **78**, 041302(R) (2008).
- [3] K. G. Lagoudakis, B. Pietka, M. Wouters, R. André, and B. Deveaud-Plédran, *Phys. Rev. Lett.* **105**, 120403 (2010).
- [4] M. Rontani and L. J. Sham, *Phys. Rev. B* **80**, 075309 (2009).
- [5] M. Abbarchi, A. Amo, V. G. Sala, D. D. Solnyshkov, H. Flayac, L. Ferrier, I. Sagnes, E. Galopin, A. Lemaître, G. Malpuech and J. Bloch, *Nat. Phys.* **9**, 275 (2013).
- [6] A. F. Adiyatullin, M. D. Anderson, H. Flayac, M. T. Portella-Oberli, F. Jabeen, C. Ouellet-Plamondon, G. C. Sallen and B. Deveaud, *Nat. Commun.* **8**, 1329 (2017).
- [7] D. Caputo, E. S. Sedov, D. Ballarini, M. M. Glazov, A. V. Kavokin and D. Sanvitto, *Nat. Photo.* **13**, 488 (2019).
- [8] B. Zenker, H. Fehske, and H. Beck, *Phys. Rev. B* **92**, 081111(R).
- [9] V. Apinyan and T. K. Kopeć, *J. Low. Temp. Phys.* **194**, 325 (2019).
- [10] For a review, see S. M. Girvin and A. H. MacDonald, *Perspectives in Quantum Hall Effects*, edited by S. Das Sarma and A. Pinczuk (Wiley, New York, 1997), Chap. V; J. P. Eisenstein, Chap. II.
- [11] For a review, see J. P. Eisenstein, *Annu. Rev. Condens. Matter Phys.* **5**, 159 (2014).
- [12] I. B. Spielman, J. P. Eisenstein, L. N. Pfeiffer and K. W. West, *Phys. Rev. Lett.* **84**, 5808 (2000).
- [13] M. Kellogg, I. B. Spielman, J. P. Eisenstein, L. N. Pfeiffer and K. W. West, *Phys. Rev. Lett.* **88**, 126804 (2002).
- [14] E. Tutuc, S. Melinte, E. P. De Poortere, R. Pillarisetty and M. Shayegan, *Phys. Rev. Lett.* **91**, 076802 (2003).
- [15] J. P. Eisenstein and A. H. MacDonald, *Nature (London)* **432**, 691 (2004).
- [16] M. Kellogg, J. P. Eisenstein, L. N. Pfeiffer and K. W. West, *Phys. Rev. Lett.* **93**, 036801 (2004).
- [17] E. Tutuc, M. Shayegan and D. A. Huse, *Phys. Rev. Lett.* **93**, 036802 (2004).
- [18] R. D. Wiersma, J. G. S. Lok, S. Kraus, W. Dietsche, K. von Klitzing, D. Schuh, M. Bichler, H.-P. Tranitz and

- W. Wegscheider, Phys. Rev. Lett. **93**, 266805 (2004).
- [19] L. Tiemann, W Dietsche, M Hauser and K von Klitzing, New J. Phys. **10**, 045018 (2008).
- [20] J.-J. Su and A. H. MacDonald, Nat. Phys. **4**, 799 (2008).
- [21] S. Misra, N. C. Bishop, E. Tutuc and M. Shayegan, Phys. Rev. B **77**, 161301(R) (2008).
- [22] O. Tieleman, A. Lazarides, D. Makogon and C. Morais Smith, Phys. Rev. B **80**, 205315 (2009).
- [23] Y. Yoon, L. Tiemann, S. Schmult, W. Dietsche, K. von Klitzing and W. Wegscheider, Phys. Rev. Lett. **104**, 116802 (2010).
- [24] A. D. K. Finck, J. P. Eisenstein, L. N. Pfeiffer and K. W. West, Phys. Rev. Lett. **106**, 236807 (2011).
- [25] D. Nandi, A. D. K. Finck, J. P. Eisenstein, L. N. Pfeiffer and K. W. West, Nature (London) **488**, 481 (2012).
- [26] D. Nandi, T. Khaire, A. D. K. Finck, J. P. Eisenstein, L. N. Pfeiffer and K. W. West, Phys. Rev. B **88**, 165308 (2013).
- [27] R. Cipri and N. E. Bonesteel, Phys. Rev. B **89**, 085109 (2014).
- [28] D. Zhang, W. Dietsche and K. von Klitzing, Phys. Rev. Lett. **116**, 186801 (2016).
- [29] I. Sodemann, I. Kimchi, C. Wang and T. Senthil, Phys. Rev. B **95**, 085135 (2017).
- [30] M. Barkeshli, C. Nayak, Z. Papić, A. Young and M. Zaletel, Phys. Rev. Lett. **121**, 026603 (2018).
- [31] J. P. Eisenstein, L. N. Pfeiffer and K.W. West, Phys. Rev. Lett. **123**, 066802 (2019).
- [32] Z. Zhu, S.-K. Jian and D. N. Sheng, Phys. Rev. B **99**, 201108(R) (2019).
- [33] D. Zhang, J. Falson, S. Schmult, W. Dietsche and J. H. Smet, Phys. Rev. Lett. **124**, 246801 (2020).
- [34] For a review, see S. M. Girvin, Int. J. Mod. Phys. B **28**, 4975 (2001).
- [35] For a review, see X. G. Wen and A. Zee, Int. J. Mod. Phys. B **17**, 4435 (2003).
- [36] Y. N. Joglekar and A.H. MacDonald, Phys. Rev. Lett. **87**, 196802 (2001).
- [37] E. Rossi, A. S. Núñez and A. H. MacDonald, Phys. Rev. Lett. **95**, 266804 (2005).
- [38] J.-J. Su and A. H. MacDonald, Phys. Rev. B **81**, 184523 (2010).
- [39] M. Titov and C. W. J. Beenakker, Phys. Rev. B **74**, 041401(R) (2006).
- [40] F. Dolcini, D. Rainis, F. Taddei, M. Polini, R. Fazio and A. H. MacDonald, Phys. Rev. Lett. **104**, 027004 (2010).
- [41] S. Peotta, M. Gibertini, F. Dolcini, F. Taddei, M. Polini, L. B. Ioffe, R. Fazio and A. H. MacDonald, Phys. Rev. B **84**, 184528 (2011).
- [42] Y.-F. Hsu and J.-J. Su, Sci. Rep. **5**, 15796 (2015).
- [43] Y.-F. Hsu and J.-J. Su, New J. Phys. **20**, 083002 (2018).
- [44] K. Moon, H. Mori, K. Yang, S. M. Girvin, A. H. MacDonald, L. Zheng, D. Yoshioka and S.-C. Zhang, Phys. Rev. B **51**, 5138 (1995).
- [45] A. A. Burkov and A. H. MacDonald, Phys. Rev. B **66**, 115320 (2002).
- [46] X.-G. Wen and A. Zee, Europhys. Lett. **35**, 227 (1996).
- [47] C. M. Pegrum, Science **312**, 1483 (2006).
- [48] K. Park and S. Das Sarma, Phys. Rev. B **74**, 035338 (2006).
- [49] X. Huang, W. Dietsche, M. Hauser and K. von Klitzing, Phys. Rev. Lett. **109**, 156802 (2012).
- [50] Y.-F. Hsu and J.-J. Su, arXiv:2006.15329.
- [51] A. A. Golubov, M. Yu. Kupriyanov and E. Il'ichev, Rev. Mod. Phys. **76**, 411 (2004).
- [52] Josephson length is a well-known characteristic length of quantum Hall bilayer exciton condensates. In this paper, its definition is given in Sec. II A.
- [53] S. Nakamura, Phys. Rev. Lett. **109**, 120602 (2012).
- [54] M. Matsumoto and S. Nakamura, Phys. Rev. D **98**, 106027 (2018).
- [55] C. Lacroix, P. Mendels and F. Mila, *Introduction to Frustrated Magnetism: Materials, Experiments, Theory* (Springer, Berlin, 2011).
- [56] P. R. Eastham, N. R. Cooper and D. K. K. Lee, Phys. Rev. B **80**, 045302 (2009).
- [57] T. Hyart and B. Rosenow, Phys. Rev. B **83**, 155315 (2011).
- [58] This inference is based on that supercurrent is proportional to the slope of the condensate phase.
- [59] H. Oda, J. Kawai, M. Miyamoto, I. Miyagi, M. Sato, A. Noguchi, Y. Yamamoto, J. Fujihira⁵, N. Natsuhara⁶, Y. Aramaki, T. Masuda and C. Xuan, Earth, Planets and Space, **68**,179 (2016).
- [60] The definition can be found in Sec. IV A.